NJC

Accepted Manuscript

This is an *Accepted Manuscript*, which has been through the Royal Society of Chemistry peer review process and has been accepted for publication.

Accepted Manuscripts are published online shortly after acceptance, before technical editing, formatting and proof reading. Using this free service, authors can make their results available to the community, in citable form, before we publish the edited article. We will replace this *Accepted Manuscript* with the edited and formatted *Advance Article* as soon as it is available.

You can find more information about *Accepted Manuscripts* in the Information for Authors.

Please note that technical editing may introduce minor changes to the text and/or graphics, which may alter content. The journal's standard Terms & Conditions and the Ethical guidelines still apply. In no event shall the Royal Society of Chemistry be held responsible for any errors or omissions in this *Accepted Manuscript* or any consequences arising from the use of any information it contains.

ROYAL SOCIETY OF CHEMISTRY

www.rsc.org/njc

Guest-induced reversible structural transitions and concomitant on/off luminescent switch of an Eu(III) metal-organic framework and its application in detecting picric acid†

Ao Li,[a] Liang Li,[a] Zhi Lin,[c] Lin Song,[a] Zi-Hao Wang,[a] Qiang Chen,[a] Tao Yang,[a] Xin-Hui Zhou,*[a] Hong-Ping Xiao*[b] and Xiu-Ju Yin[d]

[a]*Key Laboratory for Organic Electronics and Information Displays & Institute of Advanced Materials, National Jiangsu Syngerstic Innovation Center for Advanced Materials (SICAM), Nanjing University of Posts & Telecommunications, 9 Wenyuan Road, Nanjing 210023, China. E-mail: iamxhzhou@njupt.edu.cn*

[b]*College of Chemistry and Materials Engineering, Wenzhou University, Wenzhou, 325035, China. E-mail: hp_xiao@126.com*

[c]*Department of Chemistry, CICECO, University of Aveiro, 3810-193 Aveiro, Portugal.*

[d]*School of Chemistry and Biological Engineering, Hechi University, Yizhou, 546300, China.*

† Electronic Supplementary Information (ESI) available: The excitation and emission spectra, the ^{1}H NMR and ^{13}C NMR spectra, CCDC 1017739. For ESI and crystallographic data in CIF or other electronic format see DOI:

We report a flexible metal-organic framework (MOF), $(Me_2NH_2)_3[Eu_3(MHFDA)_4(NO_3)_4(DMF)_2]\cdot 4H_2O\cdot 2MeCN$ (**1**) (H_2MHFDA = 9-methyl-9-hydroxy-fluorene-2,7-dicarboxylic acid), which was synthesized by hydrothermal method and structurally characterized. This MOF has a three-dimensional framework structure with one-dimensional rhombic channels and the framework can be reversibly transformed between two phases upon release/uptake of the guest molecules. The vacuum drying process is accompanied by the loss of luminescence of MOF, while the luminescence is recovered upon resoaking in DMF. The potential of material for PA sensing was studied in DMF through the luminescence quenching experiments, which elucidates that this material is a potential turn-off luminescent sensory material for the selective detection of PA.

1. Introduction

Metal-organic frameworks (MOFs), crystalline materials constructed from metal ions and organic ligands, have been an active research area since the beginning of this century because of their functional properties and potential applications in materials science. For example, the MOFs have the potential in applications such as guest sensing and recognition because they can have a luminescent response to guest absorption and exchange.[1] The luminescent properties of MOFs are very sensitive to the environment around the chromophores, just like Eu^{3+} luminescence is a very sensitive probe of its coordination sphere. Therefore, luminescent frameworks, particularly lanthanide-based luminescent frameworks, are the most widely explored type of MOFs sensor to date, and have been used as sensors for the detection of cations and anions,[2] gases and vapors,[3] pH value[4] and temperature.[5] As well, it has been generally assumed that open metal sites in frameworks will play a crucial role in molecular recognition processes owing to their ability to impart highly selective and specific molecular transformations,[6] transport,[7] and storage.[8] In recent years, guest-sensitive properties, such as the guest-dependent luminescence of lanthanide polymers, also have become an interesting focus. However, few examples of guest-dependent luminescent property of lanthanide metal ions and luminescent response to guest molecules/anions in MOFs with structural dynamism have been reported,[9] which have a certain value for the research and application of guest sensing and recognition.

Picric acid, 2,4,6-trinitrophenol (PA) is a common ingredients of industrial explosives which even have superior explosive power than its well known counterpart 2,4,6-trinitrotoluene (TNT) at picomolar concentrations. During commercial production and use in dyes, pharmaceutical, fireworks, glass, and leather industries, PA is released into the environment, leading to the contamination of soil and aquatic systems. Therefore, the reliable and accurate detection of PA has great significance to homeland security and environmental protection.[10] However, only a few MOF materials have been synthesized, and are used in the detection of PA.[11]

Herein, based on the 9-methyl-9-hydroxy-fluorene-2,7-dicarboxylic acid

(H_2MHFDA), a high efficient Eu-based luminescent MOF $(Me_2NH_2)_3[Eu_3(MHFDA)_4(NO_3)_4(DMF)_2]\cdot 4H_2O\cdot 2MeCN$ has been prepared and structurally characterized. Although a number of Ln-MOFs have been documented, the investigations on the relationships between the crystal structures and the photoluminescence properties were relatively few. For this purpose, the structural characterizations and luminescence studies of complexes **1**, **1a** and **1b** were carried out. The results indicated that the materials exhibited framework dynamics upon several cycles of vacuum drying and resoaking in DMF solvent and a reversible large change in their luminescence intensities. It was also investigated the ability of **1b** for PA sensing in DMF through the luminescence quenching experiments. **1b** shows efficient luminescence quenching phenomena for nitro compounds,[12] especially for PA and it is a potential luminescent sensory material for nitro explosives.

Experimental Section

Syntheses

All chemicals were reagent grade and used as received. Elemental analyses for C, N and H were performed on a Perkin-Elmer 240C analyzer. Infrared spectra were recorded on a Vector22 Bruker Spectrophotometer with KBr pellets in the 400-4000 cm^{-1} regions. The powder XRD patterns were recorded on a Bruker D8-advance X-ray diffractometer equipped with Cu-Kα radiation. TGA (thermal gravimetric analysis) was collected on a Shimadzu DTG-60 under 15 mL min^{-1} nitrogen gas flow and heating rate of 5 °C/min from room temperature to 800 °C. Time-resolved fluorescence measurements were performed using a Life-Spec-ps fluorescence lifetime analytical spectrometer (Edinburgh Instruments F900). The absolute quantum yield data were collected on solid samples mounted on quartz slides. The samples were placed within an integrating sphere and excited at 340 nm. Photoluminescent spectra were measured using a RF-5301PC spectrofluorophotometer. ^{1}H and ^{13}C NMR spectra of samples in d6-DMSO were recorded at room temperature on a Bruker 400 MNMR spectrometer.

Synthesis of H_2MHFDA

The 2,7-dibromo-9-fluorenone (2.03 g, 6 mmol) was dissolved in 220 mL of dry THF, and the solution was cooled to -78 °C. The methyllithium (7.5 mL of a 12 mmol solution) was added to the solution over a period of 10 min. One hour later, the t-Butyllithium (24 mL of a 31.2 mmol solution) was added over a period of 30 min. Two hours later, the large excess of dry CO_2 was introduced for 1.5 h and then the cooling bath was removed. The suspension was stirred for 1h at room temperature and then evaporated to dryness by heating under a reduced pressure. The obtained solid was dissolved in water (90 mL), and the dichloromethane (20 mL) and concentrated hydrochloric acid (4.0 mL) was added under agitation to produce the pink solid precipitate, which was filtered off, washed with hot water, and dried at 40 °C for 12 h to give 9-methyl-9-hydroxy-fluorene-2,7-dicarboxylic acid (1.52 g, b). ^{1}H NMR (400 MHz, DMSO): δ = 8.12–8.08 (m, 2H), 8.01–7.97 (m, 2H), 7.96–7.92 (m, 2H), 5.88 (s, 1H), 1.60 (d, *J* = 14.1 Hz, 3H) (Fig. S1, Supporting Information). ^{13}C NMR (101 MHz, DMSO): δ = 167.31, 152.12, 141.62, 131.01, 130.22, 124.37, 121.07, 78.04, 25.20 (Fig. S2).

Synthesis of $(Me_2NH_2)_3[Eu_3(MHFDA)_4(NO_3)_4(DMF)_2]\cdot 4H_2O\cdot 2MeCN$ (1)

A mixture of H_2MHFDA (0.1 mmol, 28.4 mg), $Eu(NO_3)_3\cdot 6H_2O$ (0.1 mmol, 44.7 mg), DMF (5 mL), EtOH (2 mL), MeCN (1 mL) and H_2O (1 mL) was sealed in a 25 mL Teflon-lined bomb and heated at 80 °C for 3 days. The reaction mixture was slowly cooled to room temperature. Yellowish diamond-like crystals of **1** suitable for X-ray diffraction analysis were isolated in 74% yield. Elemental analysis (%) calcd for $C_{80}H_{92}Eu_3N_{11}O_{38}$: C, 42.30; N, 6.78; H, 4.08%. Found: C, 42.52; N, 7.06; H, 4.46%. IR (KBr, cm^{-1}): 542 w, 673w, 783 s, 1109 w, 1388 vs, 1429 s, 1553 s, 1589 s, 1658 s, 2927w, 3368 m.

Synthesis of $Eu_3(H_{0.75}MHFDA)_4(NO_3)_4$ ($\mathbf{1a_{170}}$)

1 was heated at 100–170 °C in a vacuum drying oven for 24 hour to obtain **1a**, in which $\mathbf{1a_{170}}$ is the 170 °C vacuum dried sample and is the fully desolvented product of **1**. Elemental analysis (%) calcd for $C_{64}H_{43}Eu_3N_4O_{32}$: C, 41.87; N, 3.05; H, 2.36%. Found: C, 41.56; N, 2.91; H, 2.54%. IR (KBr, cm^{-1}): 541 w, 673w, 783 s, 1110 w, 1388 vs, 1427 s, 1549 s, 1588 s, 1658 s, 2927 w, 3370 m.

Synthesis of $Eu_3(H_{0.75}MHFDA)_4(NO_3)_4 \cdot 5.5DMF$ (1b)

1b was obtained by soaking $\mathbf{1a_{170}}$ in DMF. Elemental analysis (%) calcd for $C_{80.5}H_{81.5}Eu_3N_{9.5}O_{37.5}$: C, 43.20; N, 5.95; H, 3.67%. Found: C, 43.51; N, 5.78; H, 3.46%. IR (KBr, cm^{-1}): 542 w, 673w, 785 s, 1109 w, 1385 vs, 1428 s, 1549 s, 1589 s, 1658 s, 2927 w, 3375 m.

X-ray crystallography

The crystal structure of complex **1** was determined on a Siemens (Bruker) SMART CCD diffractometer using monochromated Mo-$K\alpha$ radiation (λ = 0.71073 Å) at 173 K. Cell parameters were retrieved using SMART software and refined using SAINT[13] on all observed reflections. Data were collected using a narrow-frame method with scan widths of 0.30° in ω. The highly redundant data sets were reduced using SAINT[13] and corrected for Lorentz and polarization effects. Absorption corrections were applied using SADABS[14] supplied by Bruker. The structure was solved by direct method using the program SHELXS-97 and refined on F^2 by applying the full-matrix least-squares method implemented in SHELXL-97.[15] The positions of the metal atoms and their first coordination spheres were located from direct-method *E* maps; other non-hydrogen atoms were found using alternating difference Fourier syntheses and least-squared refinement cycles and, during the final cycles, were refined anisotropically. Hydrogen atoms were placed in calculated position and refined as riding atoms with a uniform value of U_{iso}. Crystallographic details have been summarized in Table 1. CCDC reference number for **1** is 1017739.

Table 1. Crystallographic data for complex **1**.

formula	$C_{80}H_{92}Eu_3N_{11}O_{38}$	Z	2
fw	2271.53	D_{calcd}, g $cm^{\cdot 3}$	1.434
crystal system	Monoclinic	T / K	173(2)
space group	$P2_1/n$	μ, $mm^{\cdot 1}$	1.848
a, Å	15.4724(19)	F(000)	2284
b, Å	14.1459(17)	reflections collected	42035
c, Å	24.040(2)	unique reflections	10337
α, deg	90.00	R_{int}, R_{sigma}	0.0130, 0.0707
β, deg	90.188(2)	GOF (F^2)	1.001

γ, deg	90.00	R_1^a,wR_2^b (I>2σ(I))	0.0543, 0.1365
V, Å^3	5261.6(10)	R_1^a,wR_2^b (all data)	0.0584, 0.1371

$R_1^a = \Sigma||F_o| - |F_c||/\Sigma|F_o|$. $wR_2^b = [\Sigma w(F_o^2 - F_c^2)^2/\Sigma w(F_o^2)]^{1/2}$.

Results and Discussion

Complex **1** was obtained by the hydrothermal reaction of H_2MHFDA and $Eu(NO_3)_3{\cdot}6H_2O$ in the mixed solvents of DMF, EtOH, MeCN and H_2O. **1** is a flexible Eu-based MOF, showing the reversible structural and optical conversions. The potential of material for PA sensing was also studied. The molecular formulas of $\mathbf{1a_{170}}$ and **1b** were confirmed by thermal gravimetric analysis and elemental analysis.

Structure of $(Me_2NH_2)_3[Eu_3(MHFDA)_4(NO_3)_4(DMF)_2]{\cdot}4H_2O{\cdot}2MeCN$ (1)

The asymmetric unit of **1** contains one and a half europium(III) ions, two MHFDA ligands, two nitrate ions, one coordinated DMF molecule, two lattice water molecules, one acetonitrile molecule, one and a half protonated dimethylamine cations, which should be obtained in situ during the solvothermal reaction due to the decomposition of DMF (Fig. 1). The Eu1 ion is eight-coordinated by seven oxygen atoms from six MHFDA ligands and one oxygen atom from one nitrate ion. The Eu2 ion is also eight-coordinated by four oxygen atoms from four MHFDA ligands, two oxygen atoms from two nitrate ions and two oxygen atoms from two terminal DMF molecules. Except the Eu1-O2 distance (2.752 Å), the Eu1–O distances are all in the range of 2.317–2.447 Å. For the Eu2 ion, there are 4 short (2.224–2.265 Å) Eu2–O_{COO} distances and 4 long (2.962–2.986 Å) Eu(2)–O_{NO_3} / O_{DMF} distances. It is suggested that there exist strong bonding interactions between Eu and MHFDA. However, the bonding interactions between Eu2 and NO_3^-/DMF are very weak. The MHFDA ligands adopt two coordination modes in **1**. One class of ligands acts as the μ_4-bridge to link four Eu ions (Eu1, Eu1^{vii}, Eu1^{viii} and Eu2, symmetry codes: ^{vii} $x - 1/2, -y + 3/2, z + 1/2$, ^{viii} $-x + 1/2, y - 1/2, -z + 3/2$) with each carboxylate oxygen atom coordinating to a Eu ion, respectively. Another class of ligands also acts in the μ_4-fashion with a carboxylate group chelating a Eu1 center and simultaneously binding to a Eu1^{i} center by a carboxylate oxygen atom. However, each oxygen atom

of another a carboxylate group bonds to a Eu ion (Eu1[ix] and Eu2[ix], symmetry code: [ix] $-x + 1/2, y + 1/2, -z + 1/2$), respectively. The Eu ions are connected by the carboxylic groups to produce the 1D parallel aligned Eu-O-C rods extending along the [010] direction. In the Eu-O-C rod, each two Eu1 ions are four-bridged by four carboxylate groups to form paddle-like dinuclear unit, and then the Eu1 ion is double-bridged to the Eu2 ion by two carboxylate groups. The Eu-O-C rods are linked along the [101] and $[\bar{1}01]$ directions by the 9-methyl-9-hydroxy-9H-fluorene moieties of the MHFDA ligands forming the three-dimensional rod-packing framework (Fig. 2) with rhombic channels running along the [010] direction, with diagonal dimensions of $a \times c$, that is 15.47 Å × 24.04 Å. The interplanar distances for (101) and $(\bar{1}01)$ crystal planes are 12.99 Å and 13.03 Å, respectively. The side length of rhombic channels is about 14.3 Å. The volume of the channels is 2788.0 $Å^3$ per unit cell or 53.0% of the total volume, calculated using the PLATON routine.[16] Nevertheless, besides the solvent molecules, they are also occupied by coordinated NO_3^- and free $Me_2NH_2^+$.

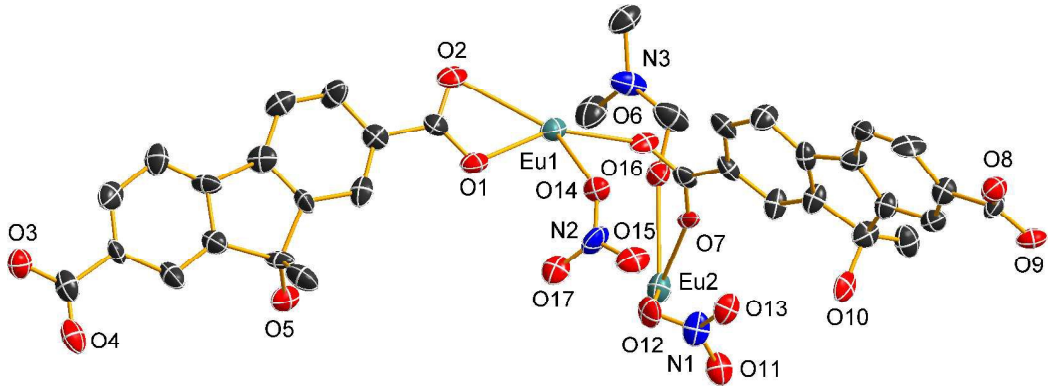

Fig. 1 View of the asymmetric unit of **1** with the thermal ellipsoids drawn at the 50% probability level. All H atoms, noncoordinated solvent molecules and $(Me)_2NH_2^+$ cation are omitted for clarity. The black ellipsoids are carbon atoms. Selected bond lengths: Eu1-O1 2.394(6), Eu1-O2 2.752(6), Eu1-O2[i] 2.392(6), Eu1-O3[ii] 2.317(6), Eu1-O6 2.317(6), Eu1-O8[iii] 2.328(6), Eu1-O9[iv] 2.329(5), Eu1-O14 2.447(5), Eu2-O4[v] 2.265(6), Eu2-O4[ii] 2.265(6), Eu2-O7 2.225(5), Eu2-O7[vi] 2.224(5), Eu2-O12 2.986(6), Eu2-O12[vi] 2.986(6), Eu2-O16 2.962(6), Eu2-O16[vi] 2.962(6). Symmetry codes: [i] $-x + 1, -y + 2, -z + 1$, [ii] $-x + 1/2, y - 1/2, -z + 1/2$, [iii] $x + 1/2, -y + 3/2, z - 1/2$, [iv] $-x + 1/2, y$

+ 1/2, –*z* + 3/2, [v] *x* + 1/2, –*y* + 3/2, *z* + 1/2, [vi] –*x* + 1, –*y* + 1, –*z* + 1.

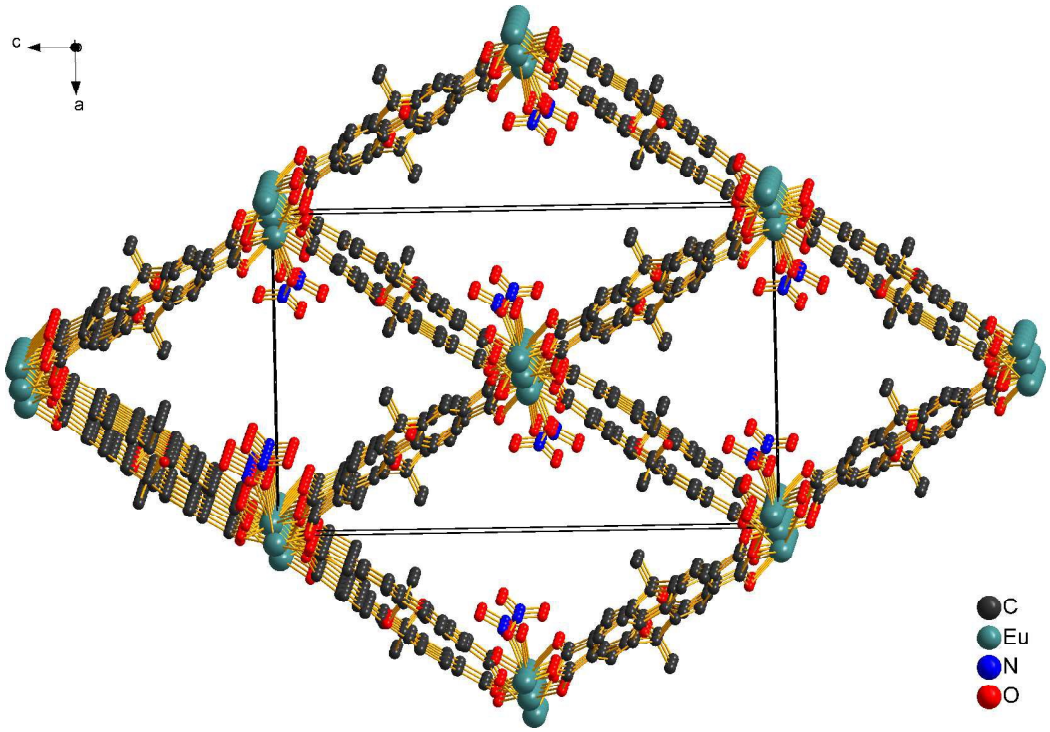

Fig. 2 The three dimensional architecture of **1**. Hydrogen atoms, DMF, MeCN, $Me_2NH_2^+$ and water molecules are omitted for clarity.

The Structural Flexibility and Thermal Stability

1 is air stable and can retain its structural integrity and keep the framework unchanged at room temperature. While **1** was heated at 100–170 °C in a vacuum drying oven for 24 hour, the framework change was observed. After vacuum drying, the strongest powder X-ray diffraction peak corresponding to the (101) and $(\bar{1}01)$ crystal planes of **1** at $2\theta_{max}$ = 6.71° disappears gradually. Simultaneously, a new strongest peak at $2\theta_{max}$ = 8.76 – 9.39 ° is observed depending on the temperature (Fig. 3). Between 50 and 100 ºC, this peak shift from 9.02 to 9.39 º. However, it appears at 8.76 º for the sample after vacuum drying at 170 º and the peak of **1** at ca. 6.71 º totally disappears. We attempted to obtain the crystal structure of vacuum dried samples, but were not successful due to many cracks appearing in crystal after vacuum drying. And only cell parameters were obtained for the 100 °C vacuum dried samples. The cell parameters are *a* = 10.5191(21) Å, *b* = 14.3737(15) Å, *c* =

26.4560(19) Å, α = 90.00°, β = 90.00°, γ = 90.00°, V = 4000.1(10) Å^3. It is interesting to compare these cell parameters with **1**. From structure point of view, the framework of **1** is formed by EuO_8 polyhedra and MHFDA links, and solvents and cations stay in the pore channels (Fig. S3). Along *b* direction, EuO_8 polyhedra are only bridged by carboxylic groups (Eu-O-C-O-Eu) while along *a* and *c* directions, EuO_8 polyhedra are connected by long organic ligands (Fig. S3). During the vacuum drying, solvents and cations were removed, coursing the shrinkage of the framework. Clearly, the deviation in *b* direction is difficult while in *a* and *c* directions it will occur due to the twist of long organic ligands. Furthermore, it is expected that *a* will shrink due to the parallelogram shape of the channel. Although **1** crystalized in monoclinic system, the β is very near 90 º. Considering that the linkage of the framework is not broken after vacuum drying at 100 ºC (see text below), it is therefore expected that the both cell may be related. In accordance with this discussion, we find that the *a* axis is shortened by 4.95 Å (shortening ratio 32%), the *b* axis almost unchanged, the *c* axis elongated by 2.42 Å (elongation ratio 10%), the cell volume shrank by 1261.5 Å^3 (shrinking ratio 24%) after vacuum drying at 100 ºC. Consequently, the rhombic window of channels becomes long-narrow, the volume of channels reduces and this narrow-pore form of the framework is designated as **1a**. Therefore, it is reasonable to assume that the axes of both systems are correlated. Analysis of the powder pattern of the sample vacuum dried at 100 ºC was further attempted using Le Bail fit.[17] However, the lack of strong peaks make the analysis difficult. Since the powder pattern is mainly related to EuO_8 polyhedra (Fig. S4), it is expected the twisted organic ligand only gives few contribution. To simplify the analysis, the space group of **1** was used and simply set the β to 90 º. The obtained results are acceptable although the quality is low (Fig. 4). The pattern of sample after 100 ºC drying can be fit using cell parameters obtained from single crystal indexing. As for pattern of sample dried at 170 ºC, only two peaks (2θ 8.76 and 17.57 º or d-space 10.07 and 5.03 Å) can clearly be seen, which are clearly related. When resoaking **1a** in the mother liquid for 12 h, the PXRD pattern nearly coincident to that observed for the as-synthesized **1** was obtained. Furthermore, the whole cycle can be repeated several times without a significant loss of

crystallinity of the material. It is suggested that the framework can be reversible transformed between two phases by guest induced.

Besides the mother liquid, we soaked **1** and **1a** in different solvents in order to check the structural transformation of the framework. In MeCN, EtOH, H_2O, MeOH, $CHCl_3$, CH_2Cl_2 and acetone, the frameworks of both **1** and **1a** collapsed to amorphous powders. In cyclohexane, *n*-butanol, *n*-propanol, N,N-dimethylacetamide (DMA), DMSO and THF, their frameworks kept unchanged. In DMF, the framework of **1** kept unchanged. However, the framework of **1a** was transformed to that of **1** in DMF, and the samples obtained by soaking $\mathbf{1a}_{170}$ (the 170 °C vacuum dried samples) in DMF are designated as **1b**. The structural transformation from **1a** to **1b** shows a very high selectivity toward DMF among other solvents.

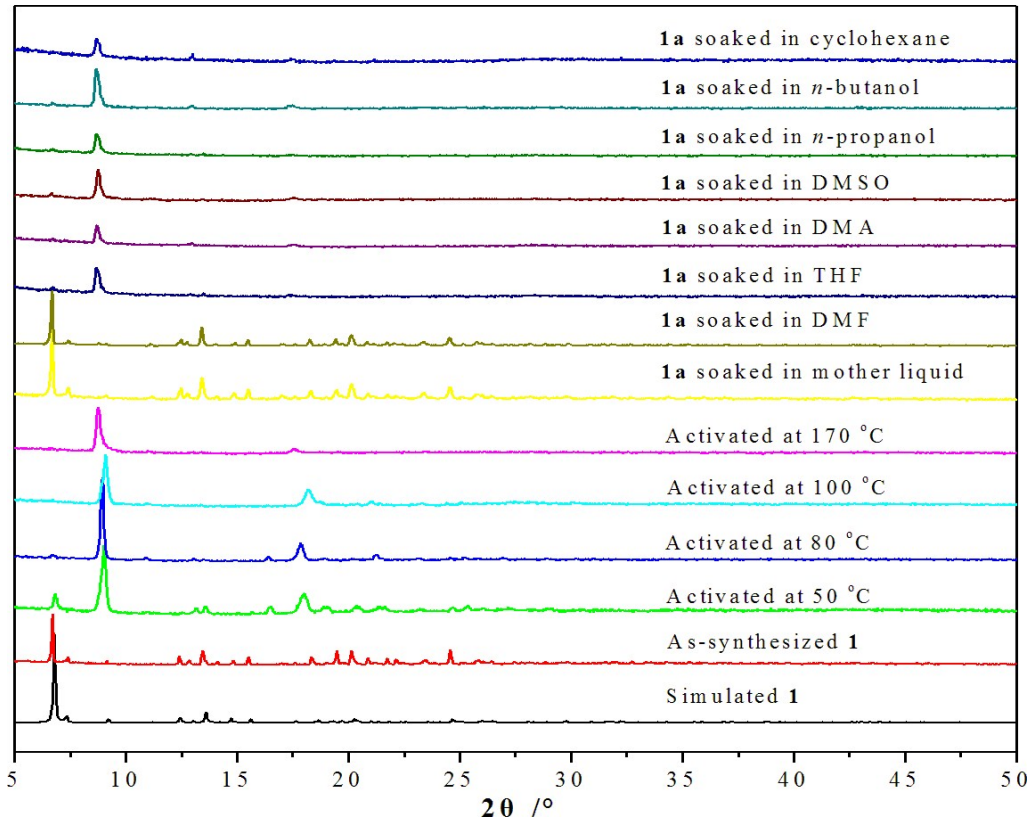

Fig. 3 The powder X-ray diffraction patterns (PXRD).

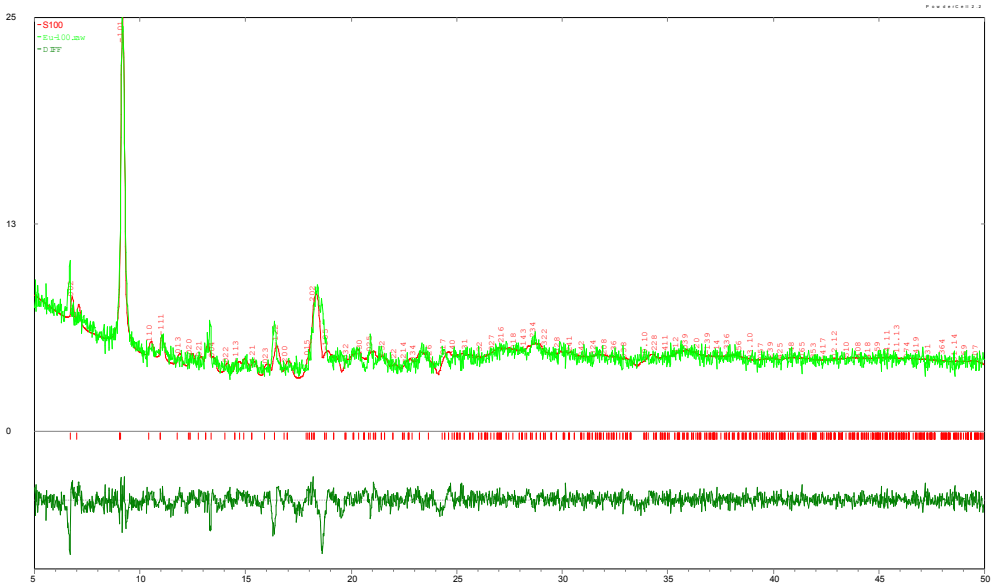

Fig. 4 Le Bail fit of powder XRD pattern of sample dried at 100 ºC using single crystal indexing parameters (a = 10.5191 Å, b = 14.3737 Å, c = 26.4560 Å, α = 90.00°, β = 90.00°, γ = 90.00°).

TGA measurements were operated at 5 °C/min and revealed that **1** undergone weight loss of 18.46% in the temperature range from room temperature to 168 °C, corresponding to the release of four water molecules, two acetonitrile molecules, two DMF molecules and three dimethylamine molecules (calculated value of 19.16%) (Fig. 5). The dimethylamines were produced by proton transfer reaction occurred between protonated dimethylamines and frameworks.[18] While in the same temperature range, the weight losses are 2.25% and zero for $\mathbf{1a_{100}}$ (the 100 °C vacuum dried samples) and $\mathbf{1a_{170}}$, respectively, which means that $\mathbf{1a_{100}}$ and $\mathbf{1a_{170}}$ are the partially and fully desolvented products of **1**, respectively. **1b** undergone weight loss of 17.88% in the temperature range from room temperature to 155 °C, corresponding to the release of 5.5 DMF molecules (calculated value of 17.96%).

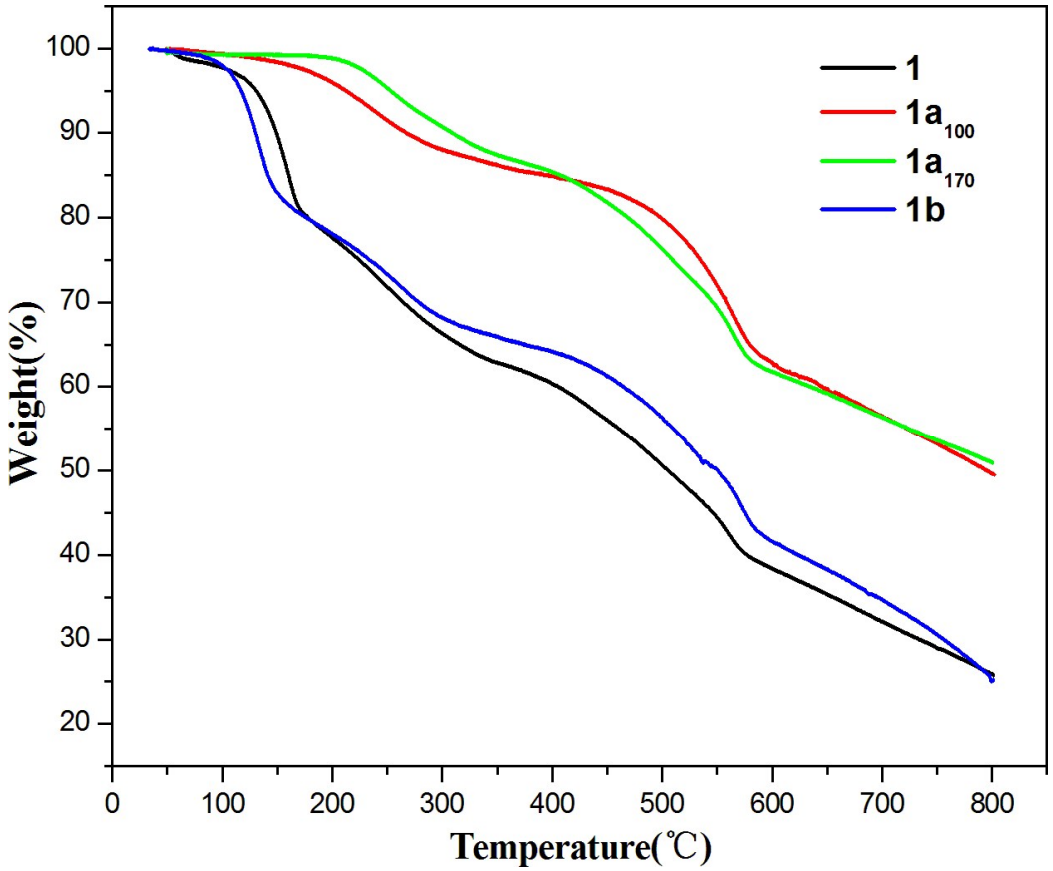

Fig. 5 Thermogravimetric curves for **1**, **1a** activated at 100 and 170°C, and **1b**.

Photoluminescent properties

When monitored under the characteristic emission (614 nm) of the Eu(III) ion, the excitation spectra of **1**, **1a** and **1b** all exhibit a broad peak with a maximum at around 340 nm (Fig. S5). **1**, **1a** and **1b** all exhibited red luminescence when excitated at 340 nm, with characteristic emissions at 579, 591, 614 with shoulder peak at 619, 652, 700 nm in the emission spectrum, corresponding to $^5D_0 \rightarrow {}^7F_J$ (J=0-4) transitions of Eu^{3+}, respectively. The blue light emission (Fig. S6) in free H_2MHFDA completely disappears and the ligands as light-harvesting chromophores (antenna effect) effectively transfer energy to Eu(III) ions. The quantum yields are 24%, 8% and almost zero for **1**, **1a**$_{100}$ and **1a**$_{170}$, respectively. The decay dynamics of the emission peak at 614 nm for **1** and **1a** can be well fitted by the biexponential curve, suggesting two emission center, which is consistent with two independent Eu(III) lattice sites in the structure. The lifetimes are τ_1 = 0.689 ms (71.6%) and τ_2 = 0.253 ms (28.4%) for **1**

(R^2 = 0.99995), τ_1 = 0.44 ms (78.1%) and τ_2 = 0.138 ms (21.9%) for **1a$_{100}$** (R^2 = 0.99995), τ_1 = 0.242 ms (32.1%) and τ_2 = 0.015 ms (67.9%) for **1a$_{170}$** (R^2 = 0.99823) (Fig. 6). These data are accordant with the luminescent intensity for **1** and **1a$_{170}$** dispersed in DMSO (3 mg/3 mL). Compared with the luminescent intensity of **1**, **1a$_{170}$** shows the very weak emission. When **1a$_{170}$** dispersed in DMF (3 mg/3 mL), the luminescent intensity is almost equal to that of **1** (Fig. S7 and S8), suggesting that luminescence recovery is accompanied by the structural transitions from **1a** to **1b**.[19]

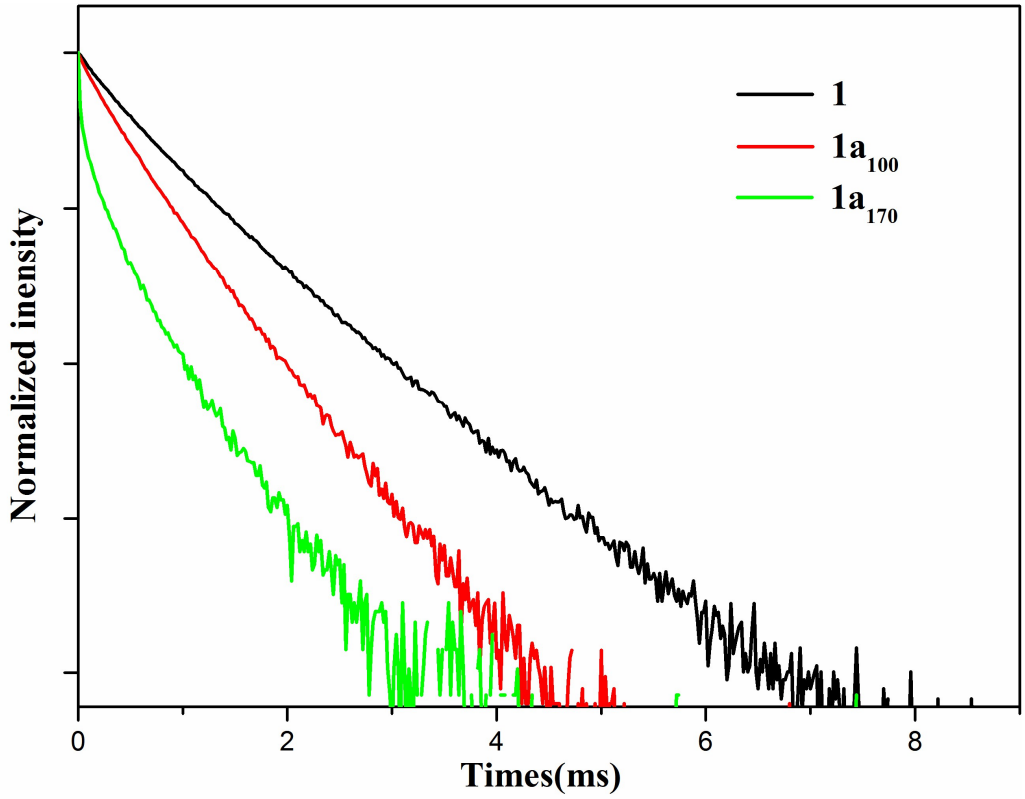

Fig. 6 Semilog plots of fluorescence decay versus time for **1** and **1a** activated at 100 and 170 °C (excited and monitored at 340 nm and 614 nm, respectively).

Detection for nitro compounds

The characteristic, bright-red luminescence and extensively aromatic structure of the host material **1b** provide the possibility of sensing target aromatic molecules via specific host–guest interactions. To explore the ability of **1b** to sense a trace quantity of nitro explosives, the luminescence responses of **1b** to various nitro compounds were investigated by addition of PA, 2,6-dinitrophenol (2,6-DNP), 2,4-dinitrotoluene (2,4-DNT), 2-nitrotoluene (2-NT), 1,2-dinitrobenzene (1,2-DNB), 1,3-dinitrobenzene

(1,3-DNB), Nitrobenzene (NB), 2,3-dimethyl-2,3-dinitrobutane (DMNB), toluene (TO) to **1b**–DMF emulsions, respectively, with the concentration of 5.0×10^{-4} M (Fig. 7). All eight nitro-compounds can weaken the photoluminescent intensity of the **1b** emulsion to varying degrees. The order of quenching efficiency is PA > 2,6-DNP > 2,4-DNT > 2-NT > 1,2-DNB > 1,3-DNB > NB > DMNB, with the largest quenching percentage (QP) of 95% for PA in DMF solution. These results demonstrate that compound **1b** has high selectivity for PA compared to other nitro compounds. Unlike the nitro compounds, an opposite effect was observed for toluene, which enhanced the luminescence emission intensity. Therefore it is speculated that the donor–acceptor electron-transfer is the dominant mechanism of luminescence attenuation and enhancement.

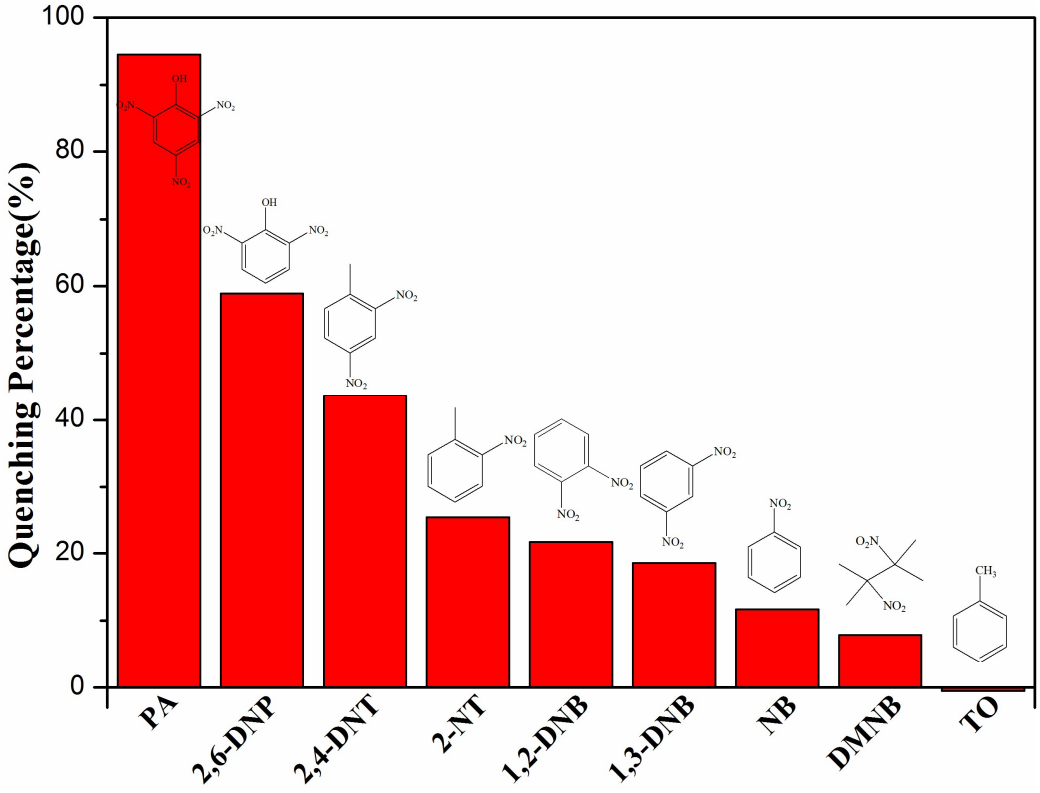

Fig. 7 Luminescence quenching percentage when **1b** was dispersed in eight different nitro compounds and toluene (TO) solutions in DMF (excited and monitored at 340 nm and 614 nm, respectively).

To better understand the high quenching efficiency of **1b** towards PA, the sensing performance was investigated in detail by the photoluminescence titration

experiments, which exhibited that upon addition of PA to **1b**-DMF emulsions, the emission intensity gradually decreased with the increase in the concentrations of the quenchers (Fig. 8). The emission of **1b** was almost completely quenched when the concentration of PA reached 1.0×10^{-3} M, showing that **1b** as a turn-off luminescent sensory material has greater sensitivity for PA. The Stern–Volmer plots of relative luminescent intensity (I_0/I) versus the PA concentration are shown in inset of Fig. 7 to further quantify the quenching efficiency, where I_0 and I are the fluorescence intensity of the emulsion in the absence and presence of PA, respectively. It is notable that the I_0/I versus PA concentration plots bend upwards instead of being the typically linear plots,[20] suggesting that the fluorescence quenching mechanism can be attributed to the presence of simultaneous dynamic and static quenching.

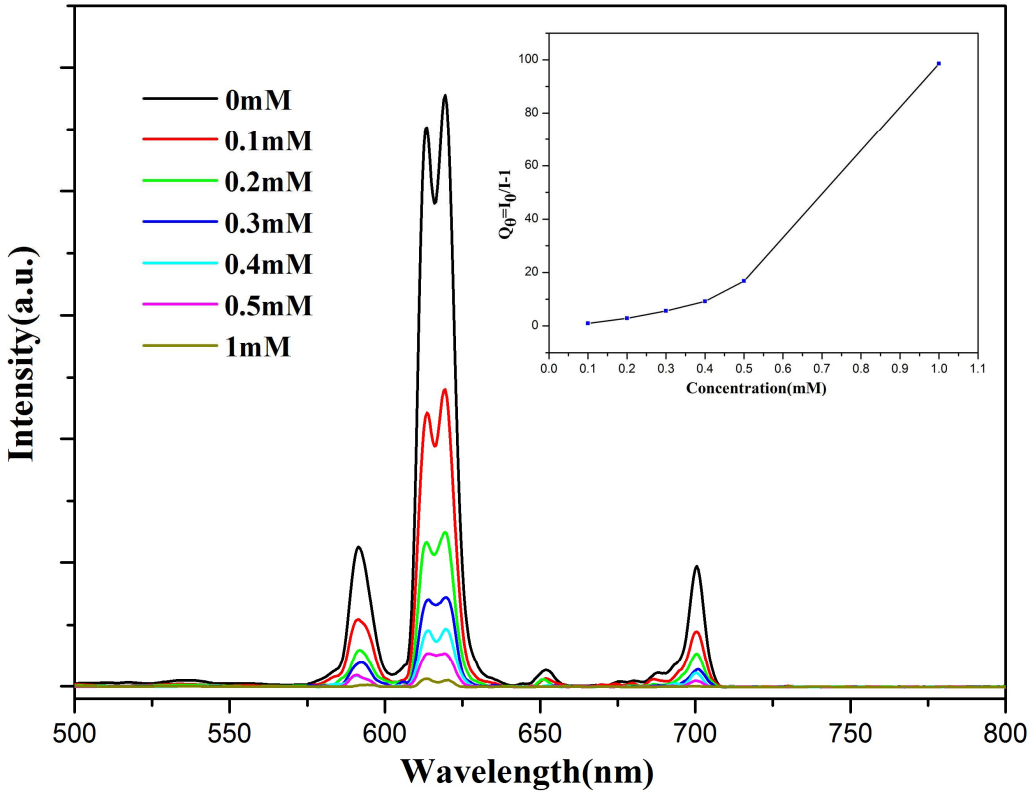

Fig. 8 Concentration-dependent luminescence quenching of **1b** (dispersion in DMF) after adding different concentrations of PA excited at 340 nm at room temperature. Inset: Stern–Volmer plot.

Conclusions

In summary, we have elucidated a novel flexible metal-organic framework which

could be reversible transformed between two phases by activated or resoaked in DMF and a reversible large change in their luminescence intensities. This unusual reverse role of DMF is probable because the environment around lanthanide ion was softened in the amorphous vacuum drying phases while it recovered stiffness upon resoak. The significant luminescence changes upon activation or resoak render the materials potential application for sensing DMF. And this understanding for the solvent induced structural transformation from this study might guide us to design and synthesize novel materials for the research and application of guest recognition and detection. The potential of **1b** for PA sensing was also investigated in DMF and its luminescent emission was turned off in the presence of PA. The fluorescence quenching mechanism for PA can be attributed to the presence of simultaneous dynamic and static quenching.

Acknowledgements

This work was supported by the National Natural Science Foundation of China (nos. 21001065, 61377019, 61136003, 21271143, 61106116 and 51173081), the Ministry of Education of China (IRT1148), Natural Science Foundation of Jiangsu Province (BM2012010), Priority Academic Program Development of Jiangsu Higher Education Institutions (PAPD) (YX03001), Specialized Research Fund for the Doctoral Program of Higher Education (SRFDP) (20113223110005), the National Basic Research Program of China (973 Program) (2012CB933301), the Project of Guangxi Education Department (YB2014331).

Notes and references

1 (a) L. E. Kreno, K. Leong, O. K. Farha, M. Allendorf, R. P. Van Duyne and J. T. Hupp, *Chem. Rev*., 2012, **112**, 1105; (b) M. Zhang, G. Feng, Z. Song, Y. Zhou, H. Chao, D. Yuan, T. T. Y. Tan, Z. Guo, Z. Hu, B. Z. Tang, B. Liu and D. Zhao, *J. Am. Chem. Soc*., 2014, **136**, 7241; (c) K. C. Stylianou, R. Heck, S. Y. Chong, J. Bacsa, J. T. A. Jones, Y. Z. Khimyak, D. Bradshaw and M. J. Rosseinsky, *J. Am. Chem. Soc*.,

2010, **132**, 4119.

2 (a) Y. Cui, Y. Yue, G. Qian and B. Chen, *Chem. Rev.*, 2012, **112**, 1126; (b) M. D. Allendorf, C. A. Bauer, R. K. Bhakta and R. J. T. Houk, *Chem. Soc. Rev.*, 2009, **38**, 1330; (c) J. He, M. Zha, J. Cui, M. Zeller, A. D. Hunter, S. Yiu, S. Lee and Z. Xu, *J. Am. Chem. Soc.*, 2013, **135**, 7807; (d) Q. Tang, S. Liu, Y. Liu, J. Miao, S. Li, L. Zhang, Z. Shi and Z. Zheng, *Inorg. Chem.*, 2013, **52**, 2799; (e) B. Manna, A. K. Chaudhari, B. Joarder, A. Karmakar and S. K. Ghosh, *Angew. Chem. Int. Ed.*, 2013, **52**, 998.

3 (a) Y. Li, S. Zhang and D. Song, *Angew. Chem. Int. Ed.*, 2013, **52**, 710; (b) G. Lu and J. T. Hupp, *J. Am. Chem. Soc.*, 2010, **132**, 7832; (c) Z. Hu, S. Pramanik, K. Tan, C. Zheng, W. Liu, X. Zhang, Y. J. Chabal and J. Li, *Cryst. Growth Des.*, 2013, **13**, 4204.

4 (a) J. Aguilera-Sigalat and D. Bradshaw, *Chem. Commun.*, 2014, **50**, 4711; (b) H. L. Jiang, D. Feng, K. Wang, Z. Y. Gu, Z. Wei, Y. P. Chen and H. C. Zhou, *J. Am. Chem. Soc.*, 2013, **135**, 13934.

5 (a) J. D. Furman, A. Y. Warner, S. J. Teat, A. Mikhailovsky and A. K. Cheetham, *Chem. Mater*., 2010, **22**, 2255; (b) X. Rao, T. Song, J. Gao, Y. Cui, Y. Yang, C. Wu, B. Chen and G. Qian, *J. Am. Chem. Soc.*, 2013, **135**, 15559.

6 X. Liu, R. J. Madix and C. M. Friend, *Chem. Soc. Rev.*, 2008, **37**, 2243.

7 (a) S. Keskin, J. Liu, R. B. Rankin, J. K. Johnson and D. S. Sholl, *Ind. Eng. Chem. Res.*, 2009, **48**, 2355; (b) L. Mi, H. Hou, Z. Song, H. Han, H. Xu, Y. Fan and S. Ng, *Cryst. Growth Des.*, 2007, **7**, 2553.

8 (a) J. L. C. Rowsell and O. M. Yaghi, *Angew. Chem. Int. Ed.*, 2005, **44**, 4670; (b) O. K. Farha, A. Ö. Yazaydın, I. Eryazici, C. D. Malliakas, B. G. Hauser, M. G. Kanatzidis, S. T. Nguyen, R. Q. Snurr and J. T. Hupp, *Nat. Chem.*, 2010, **2**, 944; (c) N. L. Rosi, J. Eckert, M. Eddaoudi, D. T. Vodak, J. Kim, M. O'Keeffe and O. M. Yaghi, *Science*, 2003, **300**, 1127; (d) L. J. Murray, M. Dincă and J. R. Long, *Chem. Soc. Rev.*, 2009, **38**, 1294.

9 (a) Y. K. Park, S. B. Choi, H. Kim, K. Kim, B. H. Won, K. Choi, J. S. Choi, W. S. Ahn, N. Won, S. Kim, D. H. Jung, S. H. Choi, G. H. Kim, S. S. Cha, Y. H. Jhon, J.

K. Yang and J. Kim, *Angew. Chem. Int. Ed.*, 2007, **119**, 8378; (b) N. Zhao, F. Sun, H. He, J. Jia and G. Zhu, *Cryst. Growth Des.*, 2014, 14, 1738.

10 Y. Salinas, R. Martínez-Máñez, M. D. Marcos, F. Sancenón, A. M. Costero, M. Parra and S. Gil, *Chem. Soc. Rev.*, 2012, **41**, 1261.

11 (a) S. S. Nagarkar, B. Joarder, A. K. Chaudhari, S. Mukherjee and S. K. Ghosh, *Angew. Chem. Int. Ed.*, 2013, **52**, 2881; (b) X. H. Zhou, L. Li, H. H. Li, A. Li, T. Yang and W. Huang, *Dalton Trans*., 2013, **42**, 12403; (c) X. Z. Song, S. Y. Song, S. N. Zhao, Z. M. Hao, M. Zhu, X. Meng, L. L. Wu and H. J. Zhang, *Adv. Funct. Mater.*, 2014, **24**, 4034.

12 (a) Z. Hu, B. J. Deibert and J. Li, *Chem. Soc. Rev.*, 2014, **43**, 5815; (b) X. H. Zhou, H. H. Li, H. P. Xiao, L. Li, Q. Zhao, T. Yang, J. L. Zuo and W. Huang, *Dalton Trans.*, 2013, **42**, 5718.

13 SAI*NT-Plus*, version 6.02; Bruker Analytical X-ray System: Madison, WI, 1999.

14 G. M. Sheldrick, *SADABSs An empirical absorption correction program*; Bruker Analytical X-ray Systems: Madison, WI, 1996.

15 G. M. Sheldrick, Acta Crystallogr., 2008, **A64**, 112.

16 A. L. Spek, *J. Appl. Crystallogr*., 2003, **36**, 7.

17 (a) A. Le Bail, H. Duroy and J. L. Fourquet, *Mater. Res. Bull.*, 1988, **23**, 447; (b) W. Kraus and G. Nolze, Federal Institute for Materials Research and Testing, Rudower Chaussee 5, 12489, Berlin, Germany.

18 Y. Wang, J. Yang, Y. Y. Liu and J. F. Ma, *Chem.Eur. J.*, 2013, **19**, 14591.

19 G. Blasse and B. C. Grabmaier, *Luminescent Materials*; Springer Verlag: Berlin, Germany, 1994; Chapter 4.

20 W. H. Zhu, Z. M. Wang and S. Gao, *Inorg. Chem.*, 2007, **46**, 1337.

GRAPHIC ABSTRACT

A flexible Eu-based MOF with strong red-light-emission exhibits the selective detection of PA among the nitro compounds.